ELECTRICAL CHARACTERISATION AND ANALYSIS OF DOMINANT CONTRIBUTIONS IN DISORDERED SEMICONDUCTING SYSTEMS WITH AN APPLICATION TO THE PURE BENTONITE MATERIAL FOR CIVIL ENGINEERING APPLICATIONS

Mohamed Essaleh✉
Geosciences, Geonvironnement and Civil Engineering Laboratory[1]
moh.essaleh@gmail.com

Rachid Bouferra
Geosciences, Geonvironnement and Civil Engineering Laboratory[1]

Soufiane Belhouideg
Research Laboratory of Physics and Engineers Sciences
Team of Applied Physics and New Technologies[2]

Mohamed Oubani
Immed-lab[1]

Abdeltif Bouchehma
Research Laboratory of Physics and Engineers Sciences
Team of Applied Physics and New Technologies[2]

Mohamed Benjelloun
Geosciences, Geonvironnement and Civil Engineering Laboratory[1]

[1]Cadi-Ayyad University
549 FSTG, B. P., Marrakech, Morocco, 40000

[2]Sultan Moulay Slimane University
592 FP, Mghila, B.P., Beni Mellal, Morocco, 23000

✉**Corresponding author**

Abstract

Semiconductors and clay materials have significant applications in environmental, civil engineering and optoelectronic sectors. The application of an electric field to such systems is subject of many works. However, to understand the behaviour of such materials under the influence of an electric field, the perception of its electrical properties is essential. In the present study, the powerful technique of complex impedance spectroscopy (CIS) is introduced to illustrate the electrical characteristics of two types of disordered semiconducting materials. These are $Cu_5In_9Se_{16}$, an ordered defect compound of the I-III-VI$_2$ family and a novel bentonite clay system which is an insulator at room temperature and semiconductor above 400 °C. Na-bentonite has been studied extensively because of its strong adsorption capacity and complexation ability while $Cu_5In_9Se_{16}$ is considered for its use in solar and phtovoltaique domain. Some of selenides have turned out to be leading materials for electro-optical devices and the tellurides for thermoelectric power generation. It is very likely that study of bentonite clay and other similar materials may lead to the technology of heterojunction and clay composite. The frequency dependence of conductivity of bentonite was investigated using an impedance analyzer in the frequency range (20 Hz – 1 MHz). The experimental data of CIS are analyzed using some analytical methods that take into account the effect of the grains and grain boundaries. The impedance data confirm the non-Debye behavior in these systems. Some important parameters related to the identified dominant contribution such as relaxation time and activation energies are estimated for the studied materials in the considered temperature and frequency ranges.

Keywords: semiconductors, Bentonite Clay material, Complex impedance spectroscopy.

1. Introduction

Semiconductors and clays are good candidates for many industrial applications and also for the understanding of carrier transport phenomena under an external electric field [1–4]. Semiconductors are used in the design and fabrication of electronic devices and integrated circuits. Also, many semiconducting materials are used for the conversion of solar energy into electrical energy [1, 2, 5, 6]. Copper ternary chalcopyrite compounds of the family of {Cu, In, Se} such as $CuInSe_2$ and $Cu_5In_9Se_{16}$ with an energy gap and high absorption coefficient of the order of 1 eV and 10^5 cm^{-1} may act as an absorber in thin film solar cell [1, 2, 7–12] devices. On the other hand, a variety of nanoparticles of semiconductors, for example TiO_2 and ZnO, can be incorporated into clay minerals. This leads to useful properties of clays for various applications, including water splitting, antibacterial activity, and photocatalysis [3, 4, 13, 14]. Moreover, semiconducting solids can be more efficient as photocatalysts instead of nanoparticles of TiO_2 and ZnO [15–17]. Bentonite is the most important industrial clay material for its applications in the environmental and civil engineering area. The physico-chemical modifications of pure bentonite have great importance in the technology of polymer semiconductors/bentonite nanocomposites [16, 17]. Complex impedance spectroscopy is a powerful technique that utilizes an alternating current (AC) signal with small amplitude, to analyze the impedance characteristics of bentonite type semiconducting materials. Theoretical models of conduction due to tunneling and hopping have been proposed to explain the frequency dependence of AC electrical conductivity [18–24]. The grain boundaries, considered as defects, tend to decrease the electrical conductivity of the system [25]. Thus, to improve the efficiency of the devices, investigation of the effect of the grain boundaries on the electrical properties of these materials is essential. The aim of this paper is to present a theoretical analysis of the frequency dependence of Z^* when the electrical conduction is governed by the contributions of the grains and grain-boundaries. Typical values of their resistances and capacitances are used in the calculation. Three analytical methods are proposed in this work to identify the dominant contributions in $Cu_5In_9Se_{16}$ that was grown by the Bridgman-Stockbarger method with a vertical multi-zone furnace [26, 27] and also in the considered pure bentonite material.

2. Materials and methods

The commercial pure bentonite powder clay was pressed into discs of about 13 mm in diameter and 2 mm in thickness by means of a hydraulic press applying pressure of 5 MPa followed by the sintering process at 800 °C for 6 h. The crystal structure of bentonite ceramics was investigated using the X-ray diffraction technique (XRD, Rigaku, smartLab) with Cu-Kα in a 2θ range from 10° to 90°, and a scan rate of 5°/min. The average crystallite size is calculated to be 61 nm. The morphological structure of bentonite was determined by the scanning electron microscope (SEM, TESCAN VEGA$_3$) coupled with the chemical microanalysis of energy dispersive X-ray spectrometry (EDX). According to the SEM and EDX analysis, the bentonite shows a porous smectite crystalline structure with a chemical formula of $(Na, Ca)_{0.3}(Al, Mg)_2Si_4O_{10}(OH)_2(H_2O)_n$ [28]. For the impedance measurement between –175 °C and –0 °C for $Cu_5In_9Se_{16}$ and 25 °C to 740 °C for bentonite, an HP-4284 A spectrometer with frequency varying between 20 Hz and 1 MHz is used. Low temperatures down to − 175 °C were performed using a liquid nitrogen cryostat, while high temperatures up to 740 °C were performed using a programmable oven.

3. Results and discussion

In disordered materials, the polarization follows the applied electric field and relaxes towards a new equilibrium state. The impedance spectroscopy allows analysis of the dominant contributions of grains and grain boundaries to the electrical conductivity in a given range of temperature and frequency. The complex modulus $M^*(M^* = M'+jM'')$ and the complex impedance $Z^*(Z^* = Z'+jZ'')$ formalisms are widely used in the literature. M^* is considered for materials with smallest capacitance while Z^* permits to identify contributions with highest resistance [29−34]. M^*, according to references 9 and 19 is expressed, in terms of Z^*, as:

$$M^* = j\omega C_0 Z^*, \qquad (1)$$

where $C_0 = \varepsilon_0 S/d$.

C_0 is the capacitance of the material in vacuum. S is the area of the electrode, d is the thickness of the sample and ε_0 is the permittivity of free space. Thus, the real and imaginary parts of M^* are expressed in terms of Z' and Z'' as follows:

$$M' = -\omega Z'' C_0 \text{ and } M'' = \omega Z' C_0. \tag{2}$$

With the contribution of the grains and grain boundaries, the equivalent circuit of a polycrystalline material is usually composed of two blocks of resistance mounted in parallel with a capacitance: $(R_g//C_g)+(R_{gb}//C_{gb})$ [34, 35].

The corresponding impedance is given by:

$$Z^* = \left(\frac{1}{R_g} + \frac{1}{Z_{C_g}} \right)^{-1} + \left(\frac{1}{R_{gb}} + \frac{1}{Z_{C_{gb}}} \right)^{-1}, \tag{3}$$

where $Z_{C_i} = \dfrac{1}{j\omega C_i}$, and

$$Z' = \left[\frac{R_i}{1+\left(R_i C_i \omega\right)^2} \right]_{i=«g»} + \left[\frac{R_i}{1+\left(R_i C_i \omega\right)^2} \right]_{i=«gb»},$$

and

$$Z'' = \left[\frac{R_i^2 C_i \omega}{1+\left(R_i C_i \omega\right)^2} \right]_{i=«g»} + \left[\frac{R_i^2 C_i \omega}{1+\left(R_i C_i \omega\right)^2} \right]_{i=«gb»}. \tag{4}$$

The corresponding calculated Bode plots for Z^* (Z' and Z'' vs. frequency) and M^* (M' and M'' vs. frequency) are represented in **Fig. 1**. In these calculations we have used some representative values of ($R_g = 2$ kΩ, $C_g = 5$ pF) and ($R_{gb} = 10$ kΩ, $C_{gb} = 100$ pF) because the order of magnitude of C_g and C_{gb} for disordered semiconducting materials is in the range 1 pF to 10 pF for C_g and 0.1 nF to 1 nF for C_{gb} [35]. In general, the grain boundaries are more resistive than the grains ($R_{gb}>R_g$). The corresponding time contant τ_g ($\tau_g = R_g C_g = 10$ ns) must lower than τ_{gb} ($\tau_{gb} = R_{gb} C_{gb} = 1$ µs) [35]. The «ZView» software is used in this work since it offers best equivalent circuit modeling and generates good quality of graphs. As shown in **Fig. 1**, Z'' as well M'' present two extrema (two minima for Z'' and two maxima for M'') at frequencies given by $f_g = (2\pi\tau_g)^{-1} = 15.9$ MHz and $f_{gb} = (2\pi\tau_{gb})^{-1} = 159$ kHz. The Nyquist diagrams (Z'' vs. Z') and (M'' vs. M'), given in the inset of **Fig. 1, a**, show two semicircles with diameters R_g and R_{gb} and two semicircles with diameters $1/C_g$ and $1/C_{gb}$ (**Fig. 1, b**). From these figures, it is possible then to conclude that M^* allows the identification of the contribution with smallest capacitance (here C_g) while Z^* permits to identify the contribution with highest resistance (here R_{gb}).

In **Fig. 2, a**, $ln(-Z'')$ and $ln(M'')$ are plotted against frequency for the previous electric circuit of two contributions $(R_g//C_g)+(R_{gb}//C_{gb})$. Here again, we can see that M'' is sensitive to the contribution located in the high frequency domain while the peak related to the contribution that lies in the low frequency domain appears better in Z''. A relatively more accurate method to determine the frequency positions of the these extrema in Z'' and M'' is to consider the second derivative of $ln(-Z'')$ and $ln(M'')$ with respect to the logarithm of frequency, $ln(f)$. This is given in the inset of **Fig. 2, a** where $d^2 ln(-Z'')/d^2 ln(f)$ and $d^2 ln(M'')/d^2 ln(f)$ present two minima at frequencies f_g and f_{gb}. This method can be used for experimental curves if the number of data is sufficiently high.

Another method to determine the frequency positions of dominant contributions is to consider the first derivative of the function $Beta = arctan(-Z''/Z')$ with respect to $ln(f)$. This is given in the inset of **Fig. 2, b** where $dBeta/dlnf$ present two maxima at frequencies f_g and f_{gb}. This method can be useful especially if the number of experimental data is not high enough. Nevertheless, the capacitances C_g and C_{gb} are replaced by constant phase elements CPE_g and CPE_{gb}, respectively, if there is a distribution of relaxation time in the material.

166
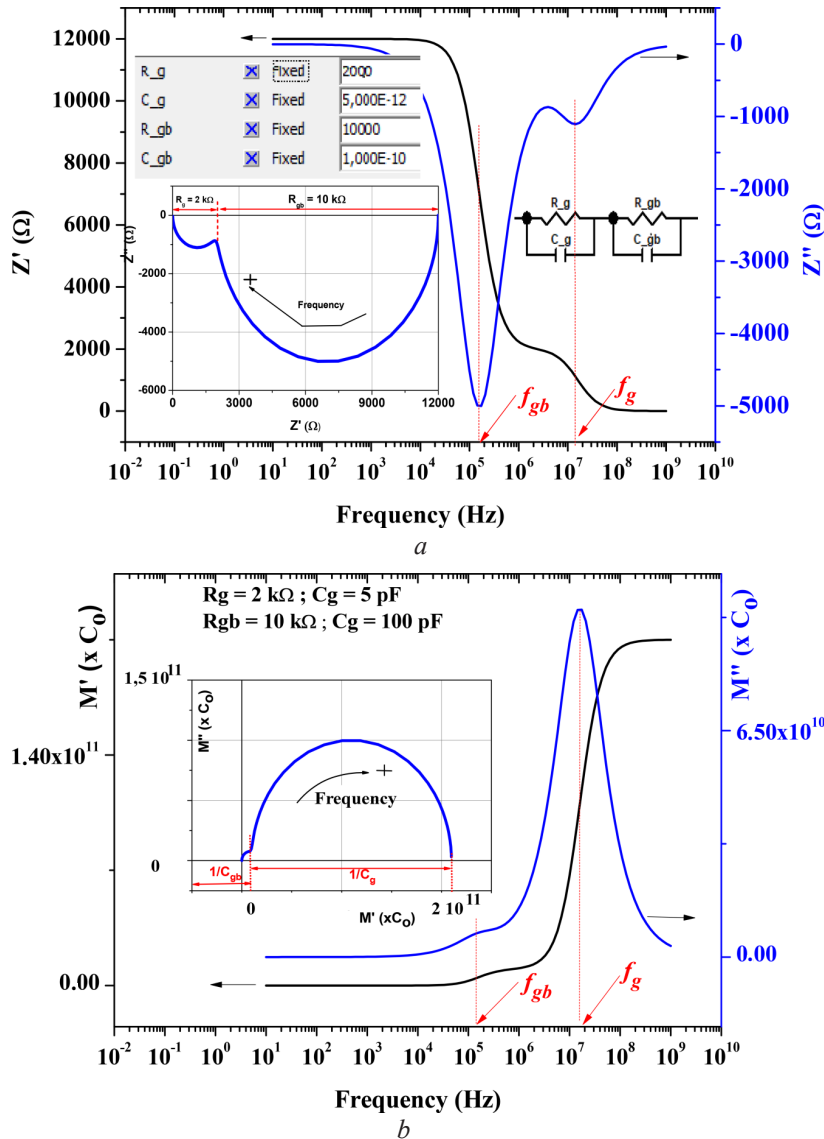
Fig. 1. Frequency dependence of impedance and modulus for an electric circuit
of two contributions $(R_g//C_g)+(R_{gb}//C_{gb})$: $a - Z'$ and Z''; $b - M'$ and M''

Their impedances are given by:

$$Z_{CPE_g} = 1/Q_g (j\omega)^{n_g}, \text{ and } Z_{CPE_{gb}} = 1/Q_{gb} (j\omega)^{n_{gb}}. \tag{5}$$

In this case (4) is replaced by the following expressions:

$$Z' = \left[\frac{R_i(1+R_iQ_i\omega^{n_i}\cos(n_i\pi/2))}{1+2R_iQ_i\omega^{n_i}\cos(n_i\pi/2)+(R_iQ_i\omega^{n_i})^2}\right] + \left[\frac{R_i(1+R_iQ_i\omega^{n_i}\cos(n_i\pi/2))}{1+2R_iQ_i\omega^{n_i}\cos(n_i\pi/2)+(R_iQ_i\omega^{n_i})^2}\right]_{i=«gb»}, \tag{6}$$

and

$$Z'' = \left[\frac{R_i^2Q_i\omega^{n_i}\sin(n_i\pi/2)}{1+2R_iQ_i\omega^{n_i}\cos(n_i\pi/2)+(R_iQ_i\omega^{n_i})^2}\right] + \left[\frac{R_i^2Q_i\omega^{n_i}\sin(n_i\pi/2)}{1+2R_iQ_i\omega^{n_i}\cos(n_i\pi/2)+(R_iQ_i\omega^{n_i})^2}\right]_{i=«gb»}. \tag{7}$$

167
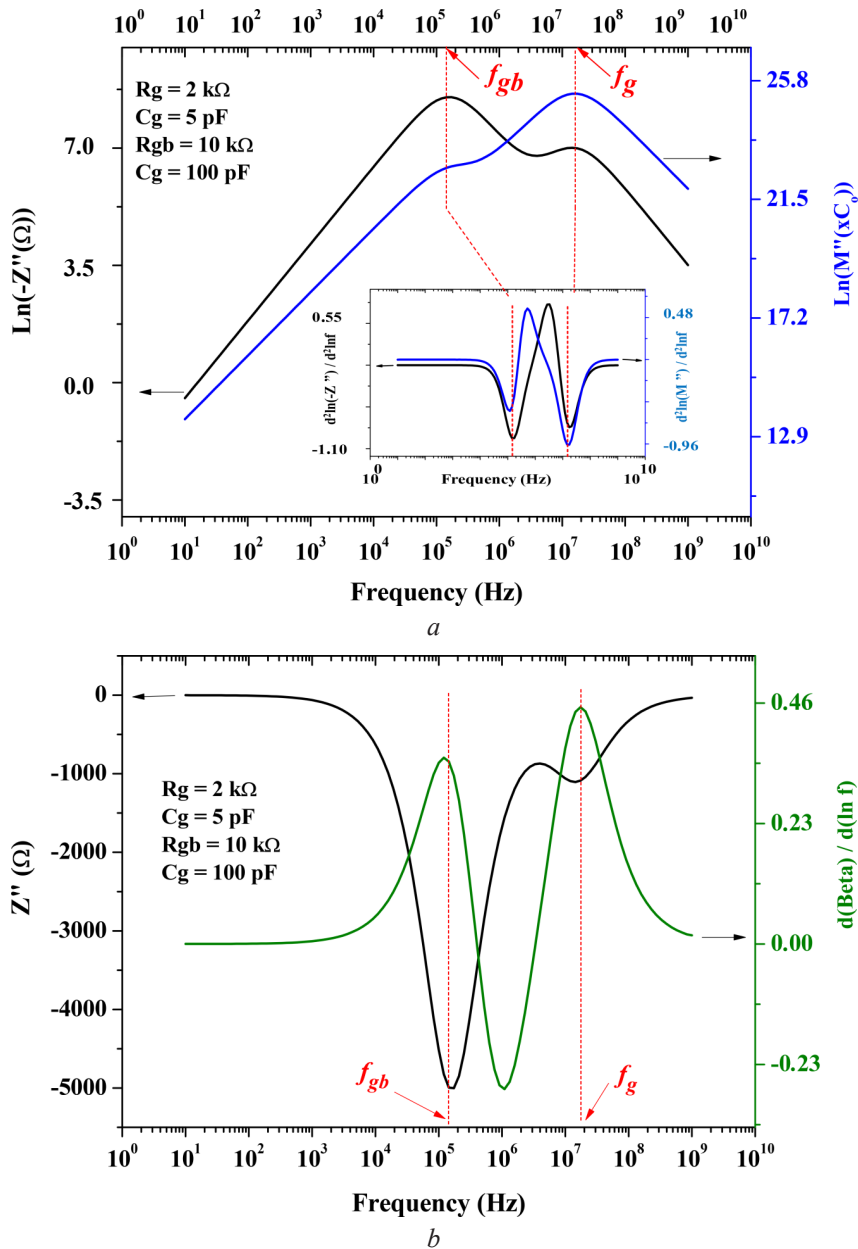
Fig. 2. Dominant contributions for an electric circuit of two bolcs $(R_g//C_g)+(R_{gb}//C_{gb})$:
a – ln$(-Z'')$ and ln(M'') with their second derivatives; b – Z'' and $dBeta/dlnf$

In these equations, Q_i is a constant which is independent of frequency. The exponent n_i measures the degree of distortion of $Z''(Z')$. This can be observed in **Fig. 3**. The value of n_i is equal to 1 for an ideal capacitor as is the case of (3). The corresponding relaxation time τ_i for each contribution «i» can be deduced from the condition $\omega\,\tau_i = 1$, where the first derivative of the function Beta $\left(\dot{\beta} = d\left(Beta\right)/dlnf\right)$ presents a maximum.

This corresponds to the equation:

$$n_i{}^2 R_i Q_i \omega^{n_i-1} \sin\left(\frac{n_i\pi}{2}\right) - n^2\left(R_i Q_i\right)^3 \omega^{3n_i-1}\sin\left(\frac{n_i\pi}{2}\right) = 0. \qquad (8)$$

(8) leads to the expression $R_i Q_i \omega^{n_i} = 1$. From this, we get:

$$\tau_g = \left(R_g Q_g\right)^{1/n_g} \text{ and } \tau_{gb} = \left(R_{gb}Q_{gb}\right)^{1/n_{gb}}. \qquad (9)$$

168

Let's now return to the material $Cu_5In_9Se_{16}$. In **Fig. 4**, we show the frequency dependence of $ln(-Z'')$ and $ln(M'')$ at a given temperature of –175 °C. Their second and also the first derivative of function *Beta* are shown in the inserts. The behavior of these derivative functions described above in **Fig. 2** indicates that the frequency position of the grain-boundary contribution is of the order of 20 kHz, while that of grains lies above 1 MHz. The latter, higher than 1 MHz, is outside the range of the present measuring equipment.
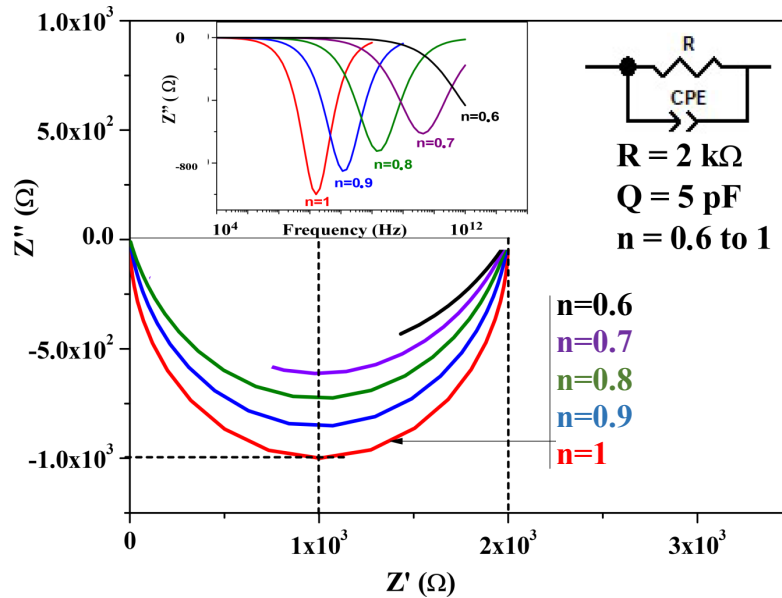
Fig. 3. Effect of the exponent n ($Z_{CPE} = 1/Q(j\omega)^n$) on the Nyquist plot (Z'' vs. Z') for an electric circuit related to one contribution ($R_g = 2$ $k\Omega$)/($C_g = 5$ pF) with the corresponding frequency dependence of Z''
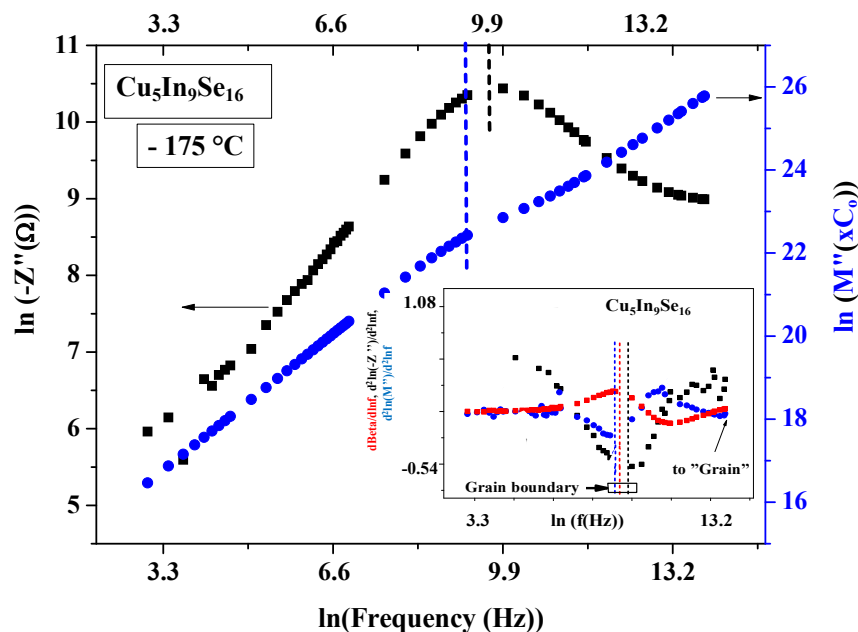
Fig. 4. Frequency dependence of $ln(-Z'')$ and $ln(M'')$ for $Cu_5In_9Se_{16}$ with their second derivatives and also the first derivative of the function Beta

The corresponding Nyquist plots (Z'' vs. Z') for Z^* and (M'' vs. M') for M^* are given in **Fig. 5**. These plots confirm the existence of the two contributions of the grains in the high frequency

domain and the grain boundaries at low frequency. Their electrical resistances are estimated to be $R_g = 38.77$ kΩ and $R_{gb} = 73.56$ kΩ (**Fig. 5, *a***).
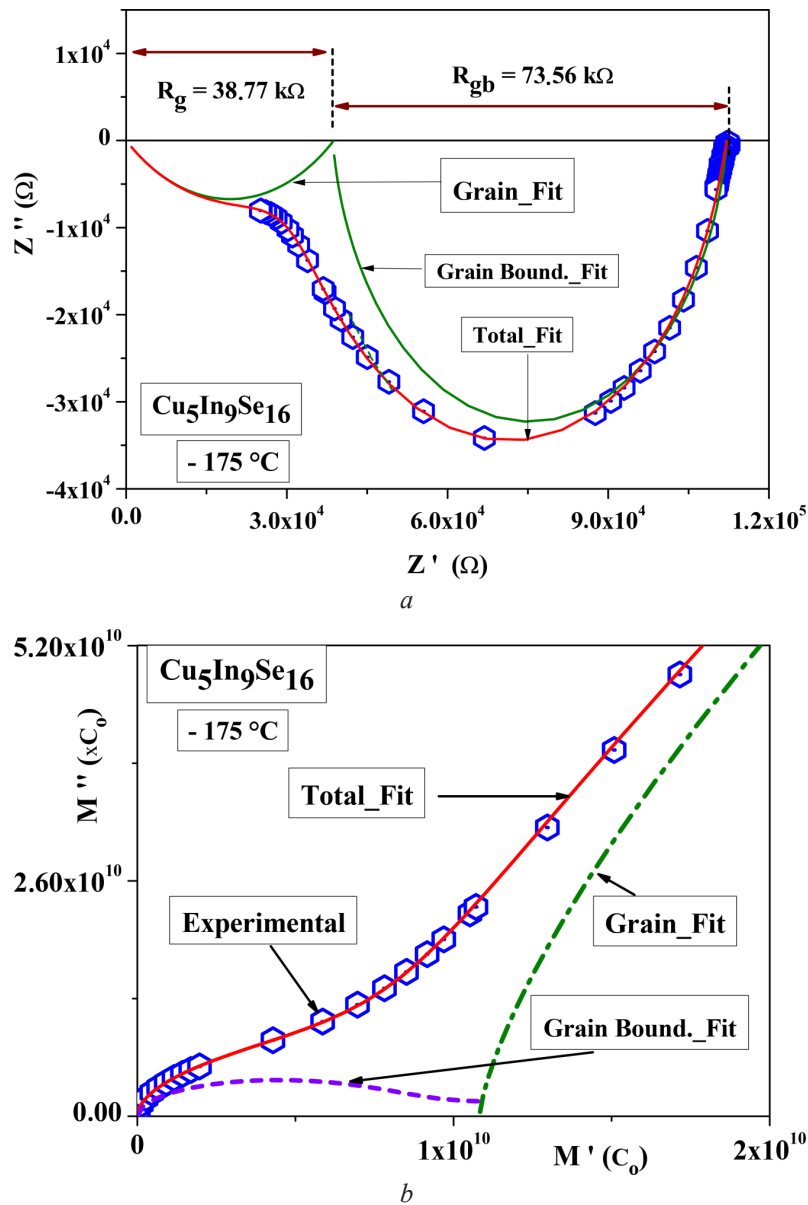
Fig. 5. The Nyquist plots of $Cu_5In_9Se_{16}$ at a representative temperature of –175 °C with the deconvolution of the grain and grain-boundary contributions: $a - Z''$ vs. Z'; $b - M''$ vs. M'

In **Fig. 6**, we represent the experimental and calculated Nyquist plots for Z^* of $Cu_5In_9Se_{16}$ according to (6), (7) at representative temperatures of – 175–165 °C, –155 °C and –145 °C. In these fits, R_g, Q_g, n_g, R_{gb}, Q_{gb} and n_{gb} are considered as adjustable parameters and their values are listed in **Table 1**. In the inset of **Fig. 6**, R_g and R_{gb} are plotted against $1/T$. From the linear fits, the activation energies for the conduction process are estimated from the corresponding slopes in the order of 22.1 and 9.2 meV for the grains and grain boundaries, respectively. The values of C_g and C_{gb} are calculated by using the expression $C_i = (R_i^{1-n_i}Q_i)^{1/n_i}$, $(i = g, gb)$ and are of the order of 10^{-12} F for the grain and 10^{-10} F for the grain boundary contribution (**Table 1**), in agreement with the literature [35]. Similar analysis of the impedance and modulus at high temperatures up to 740 °C, has been carried out for bentonite ceramic. The frequency dependence of Z', Z'', M' and M'' and their corresponding Nyquist plots are given in **Fig. 7, 8** for a given representative temperature of 500 °C.

170
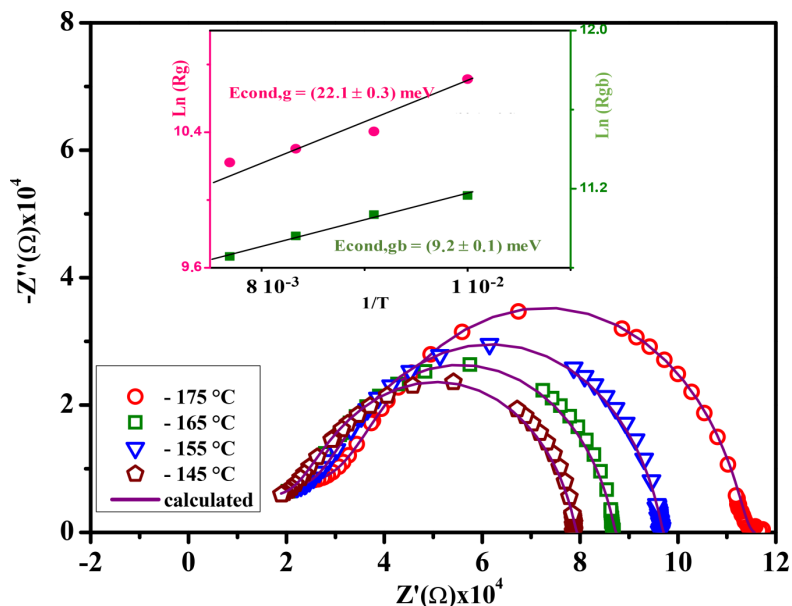
Fig. 6. Experimental and calculated Nyquist plots (Z'' vs. Z') of Cu$_5$In$_9$Se$_{16}$ at some representative temperatures with the corresponding activation energies for the conduction process

The coincidence of the peaks of Z'' and M'' (**Fig. 7**) indicates the predominance of the contribution of grains to the total electrical conduction in bentonite. Also, the minima in the second derivative of $ln(-Z'')$ and $ln(M'')$ (**Fig. 7**) take place the same frequency where the first derivative of the function $Beta$ presents a maximum. This is confirmed by the existence of only one semicircle in the Nyquist plots (**Fig. 8, a** for Z^* and **Fig. 8, b** for M^*). The best fit of the data by an electric circuit (R_g) mounted in parallel with (CPE_g) is shown in **Fig. 8** by continuous curves. The values of the adjustable parameters R_g, Q_g, and n_g used in this fit are 335.59 kΩ, 12.38 pF and 0.928.

Table 1
Values of the equivalent circuit parameters for Cu$_5$In$_9$Se$_{16}$ calculated at different temperatures

T (°C)	R_g (Ω)	Q_g ($\times 10^{-8}$)	n_g	C_g ($\times 10^{-12}$ F)	t_g ($\times 10^{-8}$ s)	R_{gb} (Ω)	Q_{gb} ($\times 10^{-10}$)	n_{gb}	C_{gb} ($\times 10^{-10}$ F)	t_{gb} ($\times 10^{-6}$ s)
−175	38770	6.336	0.36	1.889	3.981	73560	2.86	0.936	1.365	9.653
−165	33013	1.767	0.438	1.251	4.386	64111	3.72	0.908	1.268	8.130
−155	29811	1.951	0.436	1.273	4.715	57577	4.09	0.901	1.270	7.314
−145	27496	2.000	0.437	1.263	5.216	51925	4.39	0.898	1.304	6.771

The corresponding relaxation time and capacitance at 500 °C are calculated to be 1.59 µs and 4.73 pF. This obtained value of capacitance agrees with the typical value of the order of 10^{-12} F for the grains in disordered materials [35].

Finally, the microstructural evolution has a decisive effect on the physical properties of any disordered semiconducting material. Many experimental and simulation studies have been carried out to understand the microstructure which depends highly on the anisotropy of grain boundary properties such as activation energy, relaxation time, and electrical resistance [36]. The main problem is to identify the predominance of the grain-boundary contribution in the electrical conduction process in a given range of temperature. The complex impedance spectroscopy is the best method to investigate the dielectric relaxation and electrical conduction behaviors of grains and grain boundaries, which are correlated with defect behaviors [37]. In this work, we have presented some calculation methods using impedance spectroscopy data that allow to identify the predominance of the contribution of grains and/or grain-boundaries to the total electrical conduction. We have applied it to two different materials by their electrical behavior; one is conductive at very low

temperatures (around − 175 °C) and the other is conductive for temperatures higher than 400 °C up to 740 °C. This approach can be applied to any other disordered material.
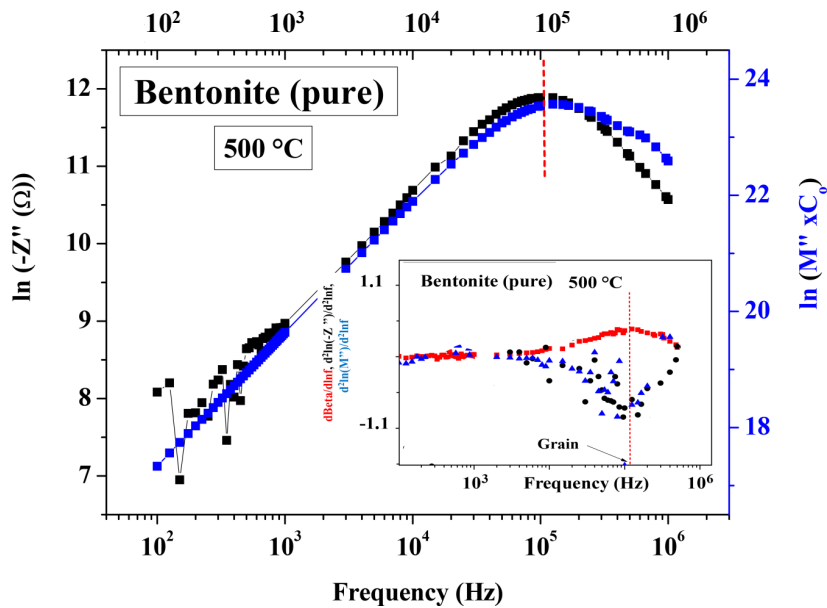
Fig. 7. Frequency dependence of $ln(-Z'')$ and $ln(M'')$ for pure bentonite with, in the inset, their second derivative and also the first derivative of Beta
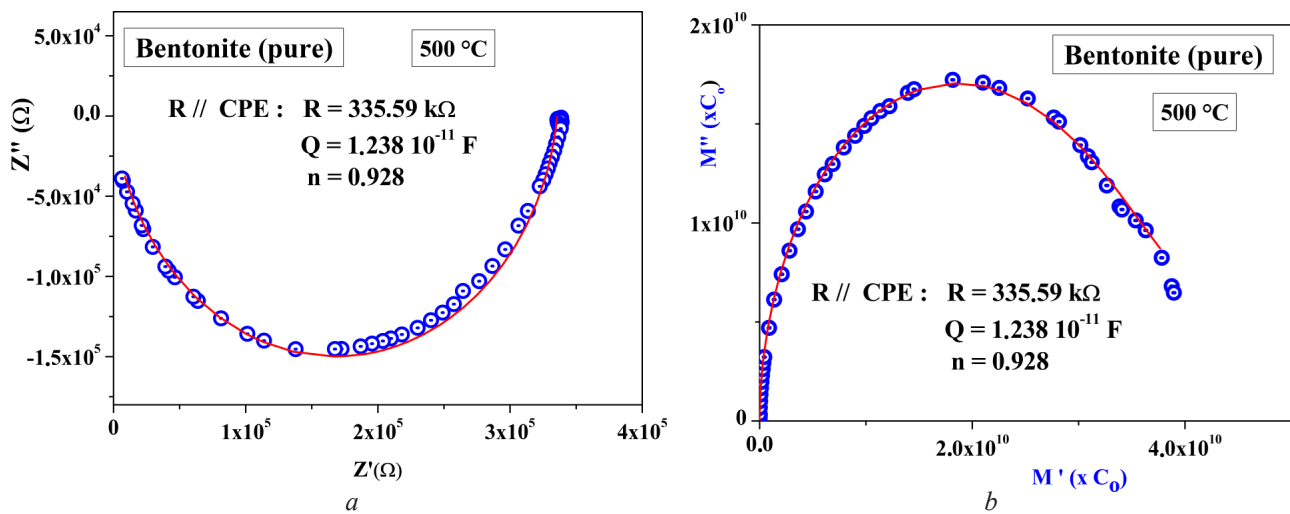
Fig. 8. Experimental and calculated Nyquist plots of bentonite at a representative temperature of 500 °C indicating the predominance of the contribution of grains in bentonite:
$a - Z''$ vs. Z'; $b - M''$ vs. M'

4. Conclusions

Analytical methods using the second derivative of $ln(-Z'')$ and $ln(M'')$ and first derivative of the function $Beta = arctan(-Z''/Z')$ are given in this work in order to identify the dominant microscopic contributions to the electrical conduction in disordered semiconducting systems. As application, we consider two materials of $Cu_5In_9Se_{16}$ at low temperatures down to –175 °C and a novel bentonite clay that becomes semiconductor at high temperatures above 400 °C with frequency between 20 Hz and 1 MHz. The magnitude of electrical resistance, capacitance, relaxation time and activation energy of grains and/or grain boundaries are determined in these materials. It is worth pointing out that intensive research of the physical properties of ternary semiconductors of the I-III-VI$_2$ family and later of their corresponding ordered defect compounds was started in the seventies. Some

of their selenides have turned out to be leading materials for electro-optical devices and solar cells and the tellurides for thermoelectric power generation. It is very likely that study of bentonite clay and other similar materials may lead to the technology of heterojunction and clay composite.

Conflict of interest

The authors declare that there is no conflict of interest in relation to this paper, as well as the published research results, including the financial aspects of conducting the research, obtaining and using its results, as well as any non-financial personal relationships.

References

[1] Sahu, M., Minnam Reddy, V. R., Park, C., Sharma, P. (2021). Review article on the lattice defect and interface loss mechanisms in kesterite materials and their impact on solar cell performance. Solar Energy, 230, 13–58. doi: https://doi.org/10.1016/j.solener.2021.10.005

[2] Nugroho, H. S., Refantero, G., Septiani, N. L. W., Iqbal, M., Marno, S., Abdullah, H. et. al. (2022). A progress review on the modification of CZTS(e)-based thin-film solar cells. Journal of Industrial and Engineering Chemistry, 105, 83–110. doi: https://doi.org/10.1016/j.jiec.2021.09.010

[3] Rakić, V., Rajić, N., Daković, A., Auroux, A. (2013). The adsorption of salicylic acid, acetylsalicylic acid and atenolol from aqueous solutions onto natural zeolites and clays: Clinoptilolite, bentonite and kaolin. Microporous and Mesoporous Materials, 166, 185–194. doi: https://doi.org/10.1016/j.micromeso.2012.04.049

[4] Horpibulsuk, S., Yangsukkaseam, N., Chinkulkijniwat, A., Du, Y. J. (2011). Compressibility and permeability of Bangkok clay compared with kaolinite and bentonite. Applied Clay Science, 52 (1–2), 150–159. doi: https://doi.org/10.1016/j.clay.2011.02.014

[5] Katariya, A., Rani, J. (2021). Review on two-dimensional organic semiconductors for thin film transistor application. Materials Today: Proceedings, 46, 2322–2325. doi: https://doi.org/10.1016/j.matpr.2021.04.401

[6] Kar, P., Shukla, K., Jain, P., Sathiyan, G., Gupta, R. K. (2021). Semiconductor based photocatalysts for detoxification of emerging pharmaceutical pollutants from aquatic systems: A critical review. Nano Materials Science, 3 (1), 25–46. doi: https://doi.org/10.1016/j.nanoms.2020.11.001

[7] Zhang, S. B., Wei, S.-H., Zunger, A., Katayama-Yoshida, H. (1998). Defect physics of the $CuInSe_2$ chalcopyrite semiconductor. Physical Review B, 57 (16), 9642–9656. doi: https://doi.org/10.1103/physrevb.57.9642

[8] Rincón, C., Wasim, S. M., Marín, G. (2002). Scattering of the charge carriers by ordered arrays of defect pairs in ternary chalcopyrite semiconductors. Applied Physics Letters, 80 (6), 998–1000. doi: https://doi.org/10.1063/1.1447597

[9] Ando, Y., Khatri, I., Matsumori, H., Sugiyama, M., Nakada, T. (2019). Epitaxial $Cu(In,Ga)Se_2$ Thin Films on Mo Back Contact for Solar Cells. Physica Status Solidi (a), 216 (16), 1900164. doi: https://doi.org/10.1002/pssa.201900164

[10] Raguse, J. M., Muzzillo, C. P., Sites, J. R., Mansfield, L. (2017). Effects of Sodium and Potassium on the Photovoltaic Performance of CIGS Solar Cells. IEEE Journal of Photovoltaics, 7 (1), 303–306. doi: https://doi.org/10.1109/jphotov.2016.2621343

[11] Heinemann, M. D., Mainz, R., Österle, F., Rodriguez-Alvarez, H., Greiner, D., Kaufmann, C. A., Unold, T. (2017). Evolution of opto-electronic properties during film formation of complex semiconductors. Scientific Reports, 7 (1). doi: https://doi.org/10.1038/srep45463

[12] Miliucci, M., Lucci, M., Colantoni, I., De Matteis, F., Micciulla, F., Clozza, A. et. al. (2020). Characterization of CdS sputtering deposition on low temperature pulsed electron deposition $Cu(In,Ga)Se_2$ solar cells. Thin Solid Films, 697, 137833. doi: https://doi.org/10.1016/j.tsf.2020.137833

[13] Terna, A. D., Elemike, E. E., Mbonu, J. I., Osafile, O. E., Ezeani, R. O. (2021). The future of semiconductors nanoparticles: Synthesis, properties and applications. Materials Science and Engineering: B, 272, 115363. doi: https://doi.org/10.1016/j.mseb.2021.115363

[14] Kumar, A., Lingfa, P. (2020). Sodium bentonite and kaolin clays: Comparative study on their FT-IR, XRF, and XRD. Materials Today: Proceedings, 22, 737–742. doi: https://doi.org/10.1016/j.matpr.2019.10.037

[15] Babu, A. T., Antony, R. (2019). Clay semiconductor hetero-system of SnO2/bentonite nanocomposites for catalytic degradation of toxic organic wastes. Applied Clay Science, 183, 105312. doi: https://doi.org/10.1016/j.clay.2019.105312

[16] Dlamini, M. C., Maubane-Nkadimeng, M. S., Moma, J. A. (2021). The use of TiO2/clay heterostructures in the photocatalytic remediation of water containing organic pollutants: A review. Journal of Environmental Chemical Engineering, 9 (6), 106546. doi: https://doi.org/10.1016/j.jece.2021.106546

[17] El-Naggar, M. E., Wassel, A. R., Shoueir, K. (2021). Visible-light driven photocatalytic effectiveness for solid-state synthesis of ZnO/natural clay/TiO2 nanoarchitectures towards complete decolorization of methylene blue from aqueous solution. Environmental Nanotechnology, Monitoring & Management, 15, 100425. doi: https://doi.org/10.1016/j.enmm.2020.100425

[18] Bilkees, R., Khan, A. A., Javed, M., Kazmi, J., Mohamed, M. A., Khan, M. N. et. al. (2021). Dielectric relaxation and variable range hopping conduction in sol-gel auto combustion derived $La_{0.7}Bi_{0.3}Fe_{0.5}Mn_{0.5}O_3$ manganite. Materials Science and Engineering: B, 269, 115153. doi: https://doi.org/10.1016/j.mseb.2021.115153

[19] Hsu, C.-C., Chou, C.-H., Jhang, W.-C., Chen, P.-T. (2019). A study of variable range hopping conduction of a sol-gel ZnSnO thin film transistor using low temperature measurements. Physica B: Condensed Matter, 569, 80–86. doi: https://doi.org/10.1016/j.physb.2019.05.036

[20] Ganaie, M., Zulfequar, M. (2021). Dielectric investigation of In4Se96-xSx semiconductor: Relaxation and conduction mechanism. Microelectronics Reliability, 116, 114018. doi: https://doi.org/10.1016/j.microrel.2020.114018

[21] Essaleh, L., Amhil, S., Wasim, S. M., Marín, G., Choukri, E., Hajji, L. (2018). Theoretical and experimental study of AC electrical conduction mechanism in the low temperature range of p-CuIn$_3$Se$_5$. Physica E: Low-Dimensional Systems and Nanostructures, 99, 37–42. doi: https://doi.org/10.1016/j.physe.2018.01.012

[22] Elliott, S. (1994). Frequency-dependent conductivity in ionically and electronically conducting amorphous solids. Solid State Ionics, 70–71, 27–40. doi: https://doi.org/10.1016/0167-2738(94)90284-4

[23] Chen, R. H., Wang, R.-J., Chen, T. M., Shern, C. S. (2000). Studies on the dielectric properties and structural phase transition of K$_2$SO$_4$ crystal. Journal of Physics and Chemistry of Solids, 61 (4), 519–527. doi: https://doi.org/10.1016/s0022-3697(99)00246-2

[24] El-Mallah, H. M. (2012). AC Electrical Conductivity and Dielectric Properties of Perovskite (Pb,Ca)TiO$_3$ Ceramic. Acta Physica Polonica A, 122 (1), 174–179. doi: https://doi.org/10.12693/aphyspola.122.174

[25] Mao, W., Xiong, B., Li, Q., Zhou, Y., Yin, C., Liu, Y., He, C. (2015). Influences of defects and Sb valence states on the temperature dependent conductivity of Sb doped SnO$_2$ thin films. Physics Letters A, 379 (36), 1946–1950. doi: https://doi.org/10.1016/j.physleta.2015.06.033

[26] Rincón, C., Wasim, S. M., Marín, G., Márquez, R., Nieves, L., Pérez, G. S., Medina, E. (2001). Temperature dependence of the optical energy gap and Urbach's energy of CuIn$_5$Se$_8$. Journal of Applied Physics, 90 (9), 4423–4428. doi: https://doi.org/10.1063/1.1405144

[27] Marín, G., Essaleh, L., Amhil, S., Wasim, S. M., Bouferra, R., Zoubir, A. et. al. (2020). Electrical impedance spectroscopy characterization of n type Cu$_5$In$_9$Se$_{16}$ semiconductor compound. Physica B: Condensed Matter, 593, 412283. doi: https://doi.org/10.1016/j.physb.2020.412283

[28] Angar, Y., Djelali, N.-E., Kebbouche-Gana, S. (2016). Kinetic and thermodynamic studies of the ammonium ions adsorption onto natural Algerian bentonite. Desalination and Water Treatment, 57 (53), 25696–25704. doi: https://doi.org/10.1080/19443994.2016.1157046

[29] Sinclair, D. C., West, A. R. (1989). Impedance and modulus spectroscopy of semiconducting BaTiO$_3$ showing positive temperature coefficient of resistance. Journal of Applied Physics, 66 (8), 3850–3856. doi: https://doi.org/10.1063/1.344049

[30] Sen, S., Pramanik, P., Choudhary, R. N. P. (2005). Impedance spectroscopy study of the nanocrystalline ferroelectric (PbMg)(ZrTi)O$_3$ system. Applied Physics A, 82 (3), 549–557. doi: https://doi.org/10.1007/s00339-005-3330-1

[31] Macedo, P. B., Moynihan, C. T., Bose, R. (1972). The Role of Ionic Diffusion in Polarization in Vitreous Ionic Conductors. Physics and Chemistry Glasses, 13, 171–179.

[32] Schneider, K., Dziubaniuk, M., Wyrwa, J. (2019). Impedance Spectroscopy of Vanadium Pentoxide Thin Films. Journal of Electronic Materials, 48 (6), 4085–4091. doi: https://doi.org/10.1007/s11664-019-07166-x

[33] Bhattacharya, G., Chaudhary, N. V. P., Adhikary, T., Aich, S., Venimadhav, A. (2021). Electron transport characteristics of FeGa, Ni/n-Si junctions by impedance spectroscopy. Superlattices and Microstructures, 156, 106958. doi: https://doi.org/10.1016/j.spmi.2021.106958

[34] Mančić, D., Paunović, V., Petrušić, Z., Radmanović, M., Živković, L. (2009). Application of Impedance Spectroscopy for Electrical Characterization of Ceramics Materials. Electronics, 13 (1), 11–17.

[35] Irvine, J. T. S., Sinclair, D. C., West, A. R. (1990). Electroceramics: Characterization by Impedance Spectroscopy. Advanced Materials, 2 (3), 132–138. doi: https://doi.org/10.1002/adma.19900020304

[36] Olmsted, D. L., Holm, E. A., Foiles, S. M. (2009). Survey of computed grain boundary properties in face-centered cubic metals – II: Grain boundary mobility. Acta Materialia, 57 (13), 3704–3713. doi: https://doi.org/10.1016/j.actamat.2009.04.015

[37] Bai, W., Chen, G., Zhu, J. Y., Yang, J., Lin, T., Meng, X. J. et. al. (2012). Dielectric responses and scaling behaviors in Aurivillius Bi$_6$Ti$_3$Fe$_2$O$_{18}$ multiferroic thin films. Applied Physics Letters, 100 (8), 082902. doi: https://doi.org/10.1063/1.3688033